J Electroceram (2009) 23:200–205
DOI 10.1007/s10832-007-9378-x

Phase evolution and Sn-substitution in $LiMn_2O_4$ thin films prepared by pulsed laser deposition

Dong Wook Shin · Ji-Won Choi · Yong Soo Cho · Seok-Jin Yoon

Received: 31 May 2007 / Accepted: 22 November 2007 / Published online: 31 May 2008

Abstract $LiMn_2O_4$ thin films prepared on a Pt/Ti/SiO_2/Si (100) substrate by pulsed laser deposition were studied with focusing on the effects of different processing conditions and Sn substitution on phase evolvement and surface microstructure. Major experimental parameters include substrate temperature up to 770 °C and working oxygen pressure of 50–250 mTorr. $LiMn_2O_4$ thin films became highly crystallized with increased grain sizes as the substrate temperature increased. Second phases such as $LiMnO_2$ and $Li_2Mn_2O_4$ were found at the temperature of 300 and 770 °C, respectively. As an optimum condition, films grown at 450 °C showed a homogeneous spinel phase with well-defined crystallinity and smooth surface. A high pressure of oxygen tended to promote crystallization and grain growth. Working pressure did not affect significantly the phase formation of the thin films except that unexpected $LiMn_3O_4$ phase formed at the lowest oxygen pressure of 50 mTorr. Tin-substituted thin films showed lower Mn–O stretching vibrations, which suggests that more Li-ions can be inserted into vacant octahedral sites of the spinel structure.

Keywords $LiMn_2O_4$ thin films · Spinel · Pulsed laser deposition · Sn substitution

D. W. Shin · J.-W. Choi (✉) · S.-J. Yoon
Thin Film Materials Research Center,
Korea Institute of Science and Technology,
Seoul 136-791, South Korea
e-mail: jwchoi@kist.re.kr

D. W. Shin · Y. S. Cho
Department of Materials Science and Engineering,
Yonsei University,
Seoul 120-749, South Korea

1 Introduction

Spinel $LiMn_2O_4$ has been reported to possess specific advantages of its low internal resistance, long cycle life, fast charging time, high cell voltage, high load current, and high thermal stability as a cathode material for lithium-ion batteries [1–7]. Particularly, sustaining the internal cell resistance at low levels is the key to obtaining a high rate-capability that has been required for the fast-charging and high-current discharging. $LiMn_2O_4$ has an inherent drawback from the unexpected phase transition of cubic spinel to tetragonal, which results from the known Jahn–Teller distortion [2, 3].

Many studies were investigated to avoid the unwanted phase transition by adopting unusual dopings or substitutions including transition metals, such as Ti, Cr, Co and Ni, and other elements, i.e., Mg and Al [4–9]. As an alternative choice, the substitution of heavy elements like W and Er were also studied with limited success due to their relatively large atomic or ionic size [10, 11].

Pulsed laser deposition has been known to be appropriate for the compositional study of thin film materials where their properties are sensitive to the small changes of substitution or stoichiometry due to the general coincidence in composition between target and deposited film. Many processing conditions designed to fabricate the PLD target, including raw materials, pellet-pressing, calcination and sintering, are known to determine the final performance of thin films by affecting stoichiometry, microstructure, oxygen deficiency and phase development [12, 13]. On the other hand, experimental parameters directly concerning the PLD process, such as substrate temperature, working pressure, laser beam power, distance between target and substrate and

Table 1 PLD processing conditions for the preparation of $LiSn_{x/2}Mn_{2-x}O_4$ thin films.

Sample ID	Target materials	Substrate temperature (°C)	Working pressure (mTorr)	Sample/target distance (cm)	PLD power (mJ)	Deposition time (min)
PL-1	$LiMn_2O_4$	RT	200	4	160	45
PL-2	$LiMn_2O_4$	300	200	4	160	45
PL-3	$LiMn_2O_4$	450	200	4	160	45
PL-4	$LiMn_2O_4$	600	200	4	160	45
PL-5	$LiMn_2O_4$	770	200	4	160	45
PL-6	$LiMn_2O_4$	450	50	4	160	45
PL-7	$LiMn_2O_4$	450	100	4	160	45
PL-8	$LiMn_2O_4$	450	250	4	160	45
PL-9	$LiMn_2O_4$	300	240	3.3	300	30
PL-10	$LiMn_2O_4$	300	150	4	300	10
PSL-1	$LiSn_{0.0125}Mn_{1.975}O_4$	450	200	4	160	45
PSL-2	$LiSn_{0.025}Mn_{1.95}O_4$	450	200	4	160	45

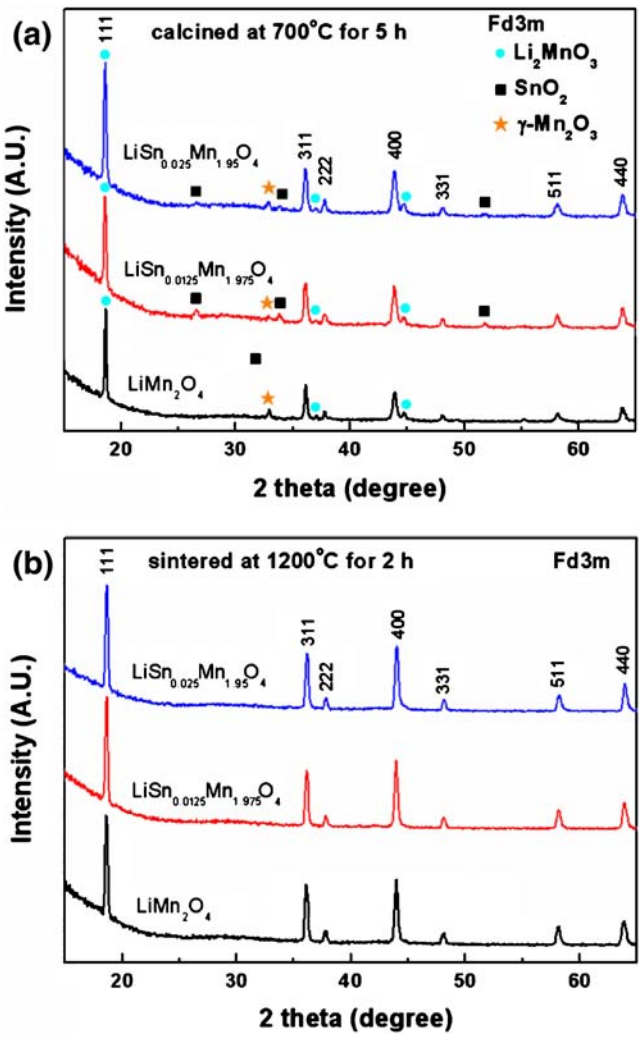

Fig. 1 XRD patterns of target materials of $LiSn_{x/2}Mn_{2-x}O_4$ (x=0, 0.025 and 0.05) (**a**) after calcining at 700 °C for 5 h and (**b**) after sintering at 1200 °C for 2 h

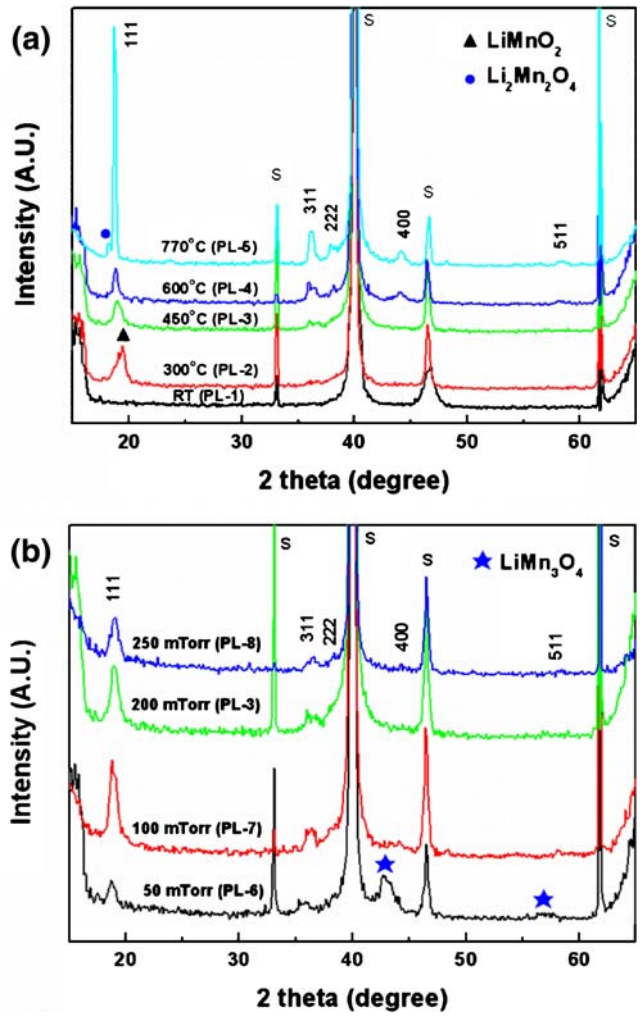

Fig. 2 XRD patterns of the $LiMn_2O_4$ thin films prepared at (**a**) different substrate temperatures (room temperature, 300, 450, 600, 770 °C) and (**b**) different oxygen pressures (50, 100, 200, 250 mTorr; *S* corresponds to substrate peaks)

deposition time, are critical for desirable performance of thin films [14–17].

In this preliminary work, deposition conditions of unsubstituted $LiMn_2O_4$ thin films prepared by PLD were investigated to initially optimize substrate temperature and oxygen pressure in terms of phase involvement and microstructural characteristics. In addition, the effects of Sn substitution as represented in the film composition of $LiSn_{x/2}Mn_{2-x}O_4$ (x=0, 0.025 and 0.05) were investigated by the analytical techniques including XRD, SEM and Raman spectroscopy.

2 Experimental

2.1 Preparation of targets

The pure $LiMn_2O_4$ and tin-substituted $LiSn_{x/2}Mn_{2-x}O_4$ (x= 0.025 and 0.05) targets were prepared by using the conventional solid state reaction method. Corresponding raw materials of Li_2CO_3 (>99%, Aldrich), MnO_2 (>99%, Aldrich) and SnO (>99%, Aldrich) were mixed by ball-milling in anhydrous ethanol for 20 h. The powder mixture was completely dried at 120 °C, grounded in an alumina

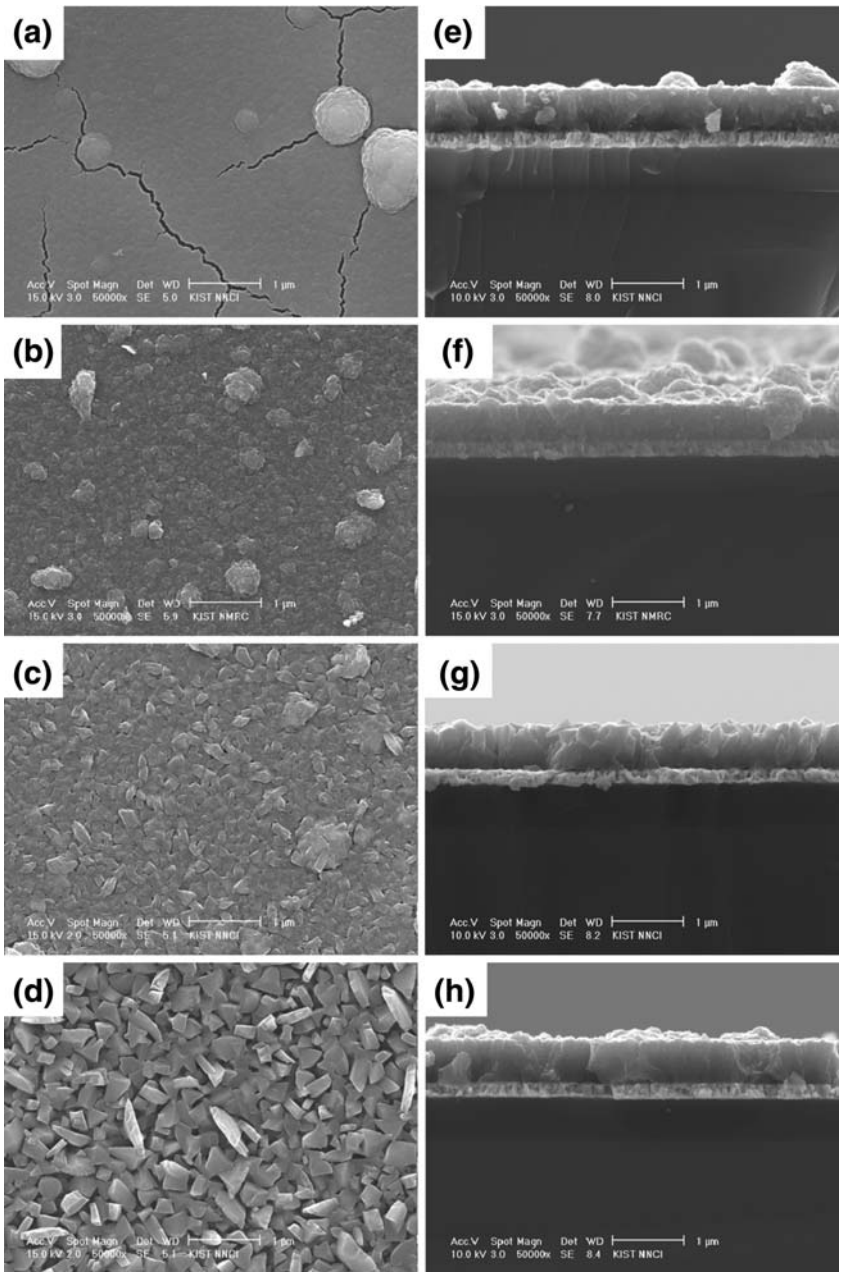

Fig. 3 SEM images for surface and cross-section of $LiMn_2O_4$ thin film prepared at the substrate temperature of (**a**, **e**) room temperature, (**b**, **f**) 450, (**c**, **g**) 600 and (**d**, **h**) 770 °C at the fixed oxygen pressure of 200 mTorr

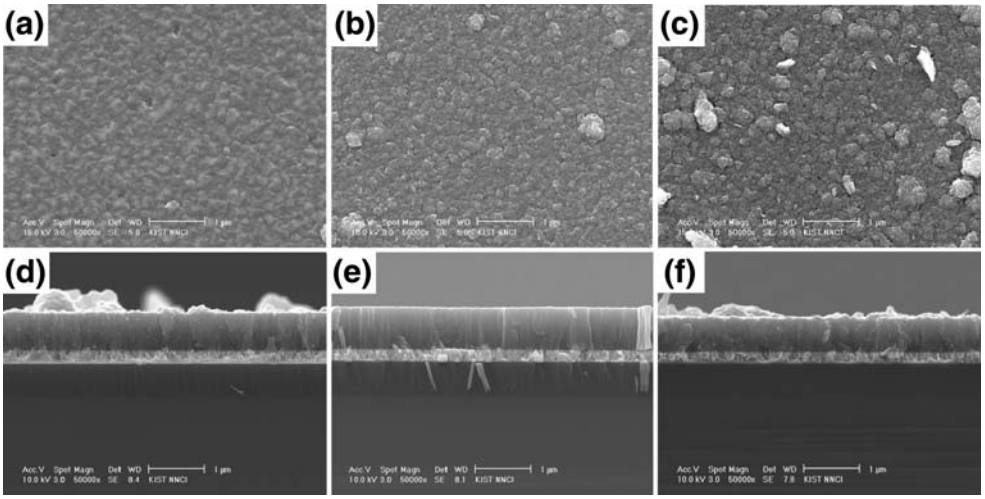

Fig. 4 Surface and cross-sectional microstructures of $LiMn_2O_4$ thin films prepared at working pressure of (**a**, **d**) 50, (**b**, **e**) 100 and (**c**, **f**) 250 mTorr and at the fixed substrate temperature of 450 °C

mortar, and then calcined at 700 °C for 5 h. The calcined power was grinded again and then uniaxially pressed at 5 ton/cm^2. Finally, the pressed specimens were sintered at 1200 °C for 2 h. The fired targets were characterized as a fired density of ~3.5 g/cm^3 (~80% of the theoretical) and a shrinkage of −1% regardless of target compositions.

2.2 Preparation of thin films

$LiSn_{x/2}Mn_{2-x}O_4$ (x=0, 0.025 and 0.05) thin films were prepared on Pt/Ti/SiO_2/Si(100) substrate at different temperatures and working pressures by pulsed laser deposition method. Table 1 represents the sample ID and processing conditions such as substrate temperature, working pressure, target/sample distance, the PLD power and deposition time. A KrF excimer laser beam (248 nm) with the pulse power of 160 to 300 mJ and the pulse repetition frequency of 10 Hz was focused on the prepared $LiSn_{x/2}Mn_{2-x}O_4$ targets. The base pressure of the vacuum chamber was below 1×10^{-5} Torr and the working pressure, determined by oxygen gas flow, was in the range of 50 to 250 mTorr. The substrate to target distance was either 3.3 or 4 cm. The pure $LiMn_2O_4$ thin films were deposited at the substrate temperatures of room temperature (RT) to 770 °C. For the Sn-substituted thin films, a fixed PLD condition of 450 °C and 200 mTorr were used. The films were grown while the target was rotating at 12 rpm.

2.3 Characterization

A Rigaku RINT 2000 X-ray diffractometer (Rigaku Ltd., Japan) using Cu Kα radiation was used for identification of crystalline phase. The surface and cross-sectional microstructures of the films were observed using a FEI XL-30 field-emission scanning electron microscope. Raman spectroscopy was used at room temperature in air with a double monochromator (Jobin-Yvon U1000) using the 514.5 nm line of an argon-ion laser (Coherent Innova 70) at a power level of 20 mW. The laser spot size at the surface of the sample was about 100 nm^2. The signal was detected with a photomultiplier and a standard photon-counting system.

3 Results and discussion

Figure 1 shows the X-ray diffraction patterns of $LiSn_{x/2}Mn_{2-x}O_4$ targets before and after sintering at 1200 °C for 2 h. Although some impurity phases like Li_2MnO_3, SnO_2 and γ-Mn_2O_3 were shown just after calcining raw materials at 700 °C for 5 h, only $LiMn_2O_4$-based spinel (Fd3m) phase was found after sintering the $LiSn_{x/2}Mn_{2-x}O_4$ targets at 1200 °C for 2 h regardless of Sn substitution. This suggests that Sn can be incorporated into the spinel structure through the sintering process.

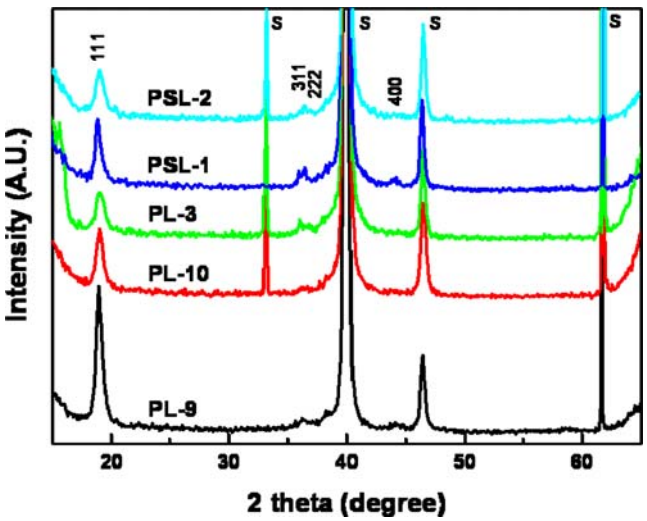

Fig. 5 XRD patterns of the pulsed-laser deposited $LiSn_{x/2}Mn_{2-x}O_4$ thin films (*S* corresponds to substrate peaks)

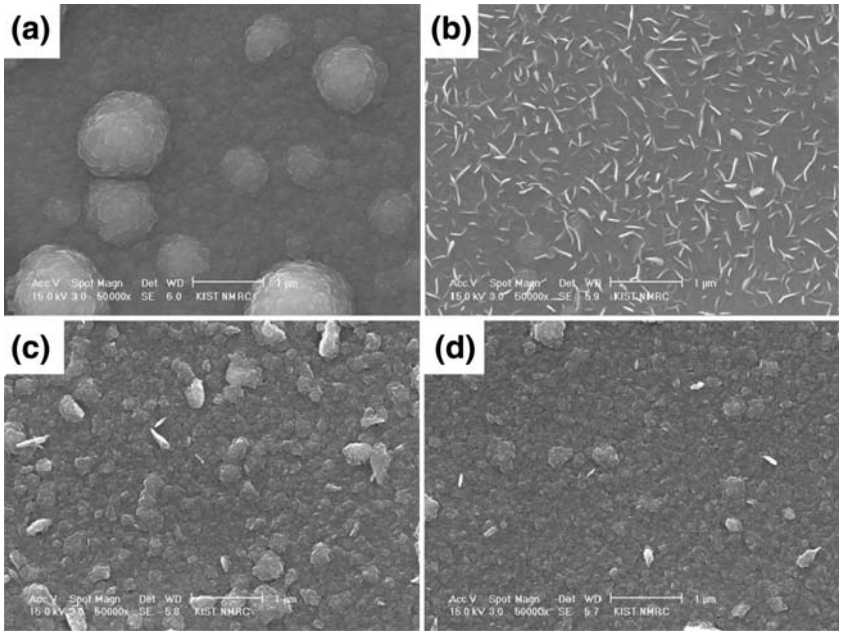

Fig. 6 Surface microstructures of (**a**) PL-9, (**b**) PL-10, (**c**) PSL-1 and (**d**) PSL-2

Figure 2(a) shows the dependence of substrate temperature on the phase development of pure $LiMn_2O_4$ thin films. Single spinel phase of $LiMn_2O_4$ was found to be stable at the temperatures of 450 to 600 °C. A second phase of $LiMnO_2$ was observed at the lower temperature of 300 °C while lithium-rich $Li_2Mn_2O_4$ at the higher temperature of 770 °C. In the temperature range of 300 to 770 °C, specifically, the peaks of the spinel $LiMn_2O_4$ phase tended to shift continuously to the lower degree. It strongly suggests that increasing temperature beyond the critical one intensifies the level of Li involvement as reported in the literature where dominant Li incorporation was observed in the pulsed laser deposited $LiMn_2O_4$ thin films [18].

Figure 2(b) shows the effects of working pressure on the phase development of the pure $LiMn_2O_4$ thin films. There was no change in the phase identification and peak shifts at the working pressures higher than 50 mTorr. Only the unexpected $LiMn_3O_4$ impurity phase was observed at the extremely low pressure of 50 mTorr.

Figures 3 and 4 show the surfaces and cross-sections of the $LiMn_2O_4$ thin films prepared at different substrate temperatures and oxygen pressures which correspond to the XRD conditions of Fig. 2. The overall tendency of microstructural changes with increasing substrate temperature (Fig. 3) agrees well with the observed change in the degree of crystallinity of the spinel phase with temperature starting from the amorphous state as seen in Fig. 2(a). There are apparent cracks at room temperature induced before the actual densification at high temperatures. The cracks disappeared as temperature increased above 450 °C. The thin films grown at 450 °C showed the most promising characteristics such as smoother surface and less voids. At high temperatures above 600 °C, crystallization seemed to progress considerably and leads to a distinct grain structure. Grain size and the degree of surface roughness must depend on substrate temperature as evidenced in the enlarged grains and rougher surface of the microstructure at 770 °C. The thickness of each film did not change significantly with substrate temperature as shown in Fig. 3. The value was near 600 nm.

The microstructures of samples according to working pressure were observed as shown in Fig. 4. A less developed grain structure was found at 50 mTorr. The working pressure of 100 mTorr seemed to produce the

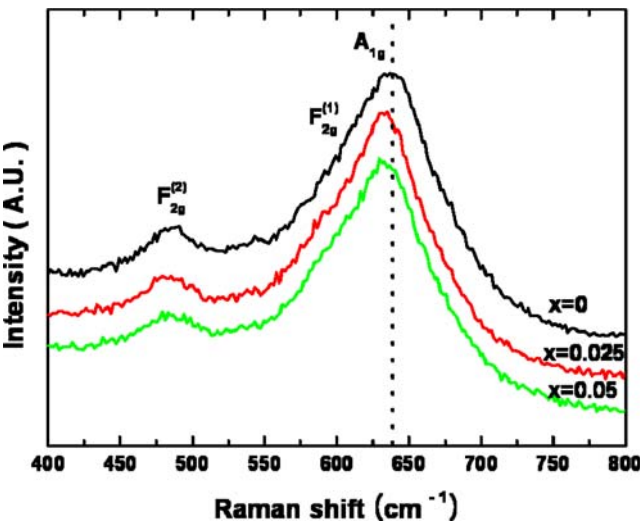

Fig. 7 Raman scattering spectra of $LiSn_{x/2}Mn_{2-x}O_4$ (x=0, 0.025 and 0.05) thin films

optimal microstructure in terms of surface cleanliness and smoothness although it is believed that the working pressure does not influence significantly the characteristics of film microstructure as long as a working pressure above 100 mTorr is used. The thickness of thin film deposited at 50 and 100 mTorr is larger than that deposited at 200 and 250 mTorr because a pulsed laser plume spreads widely at low oxygen pressures whereas the plume is restricted by high oxygen pressures.

Other processing conditions to see the effects of PLD power, sample/target distance and deposition time were also applied to the preparation process of the pure and tin-substituted thin films as seen in the designated samples of PL-9, PL-10, PSL-1 and PSL-2 in Table 1. Independently on PLD power and deposition time, the XRD analysis of Fig. 5 shows only $LiMn_2O_4$-based spinel phase and the (111) preferred orientation for all samples. Figure 6 shows the surface morphology of the thin films having various conditions corresponding to Fig. 5. Large particles in Fig. 6(a) are generally thought to be derived from a high oxygen pressure and high power collisions onto the target. Figure 6(b) shows that bean-pod shape grains appeared at a low working pressure even though the thin film has been deposited at a high PLD power. The bean-pod shape grain is known to be not really crystals but belongs to transition states between amorphous and crystals [15].

An optimized PLD condition of substrate temperature ~450 °C, working pressure ~200 mTorr, target/substrate distance ~4 cm, PLD power ~160 mJ, deposition time ~45 min was applied for the preparation of $LiSn_{x/2}Mn_{2-x}O_4$ (x=0.025 and 0.05) thin film as PSL-1 and PSL-2 in Table 1. The deposition rate was comparable as 10–15 nm/min regardless of target composition. It seemed that the substitution of Sn did not change significantly the surface microstructures of thin films as compared between Fig. 3(b) and Fig. 6(c,d).

Figure 7 shows the Raman spectra of $LiSn_{x/2}Mn_{2-x}O_4$ thin films deposited at the PLD condition used for PL-3, PSL-1 and PSL-2. Raman scattering is able to probe the near-neighbor environment of oxygen coordination around the Mn ions. The main peak around 630 to 650 cm^{-1} shows the Mn–O stretching vibration of spinel structure. The main A_{1g} peaks of tin-substituted thin films shifted to the lower Raman values, which suggests that the Mn–O stretching vibrations decreased by tin substitution [16, 19, 20]. The decreased Mn–O stretching vibration means that the Mn–O bond is shortened in the spinel structure by the tin substitution. Because of the shortened Mn–O bond, it is expected that more lithium ions can be inserted into the vacant octahedral sites of the spinel without a phase transition and its structural stability can be enhanced. Moreover, the shortness of Mn–O bond possibly enlarges the space of 16c octahedral sites in spinel.

4 Conclusions

In this study of $LiSn_{x/2}Mn_{2-x}O_4$ thin films prepared by pulsed laser deposition, phase evolution and resultant microstructures were found to strongly depend on the processing conditions such as substrate temperature and working pressure. Unexpected phases, of $LiMnO_2$, $Li_2Mn_2O_4$ and $LiMn_3O_4$, which are deviating from the normal spinel $LiMn_2O_4$ phase, were observed to be developed at the extreme temperature or oxygen pressure as a distinguishable feature of this study. These unwanted phases could be avoided by controlling the processing parameters. For example, an acceptable range of substrate temperature was regarded as 450 to 600 °C as pure spinel phase was found in this temperature range. The optimal processing condition could be successfully applied to the Sn-substituted $LiMn_2O_4$ thin films. The effect of Sn substitution can be highlighted as a lower Mn–O stretching vibration, which is presumably associated with the intercalation of Li into the vacant octahedral sites in the spinel structure.

References

1. N.J. Dudney, J.B. Bates, R.A. Zuhr, S. Young, J.D. Robertson, H.P. Jun, S.A. Hackney, J. Electrochem. Soc. **146**(7), 2455 (1999)
2. R.J. Gummow, A. de Kock, M.M. Thackeray, Solid State Ion. **69**, 59 (1994)
3. J.M. Tarascon, E. Wang, F.K. Shokoohi, J. Electrochem. Soc. **138** (10), 2859 (1991)
4. Y.J. Park, M.M. Doeff, J. Power Sources **165**, 573 (2007)
5. M. Kaneko, S. Matsuno, T. Miki, M. Nakayama, H. Ikuta, Y. Uchimoto, M. Wakihara, K. Kawamura, J. Phys. Chem. B **107**, 1727 (2003)
6. H.S. Moon, J.W. Park, J. Power Sources **119**, 717 (2003)
7. Y.J. Wei, L.Y. Yan, C.Z. Wang, X.G. Xu, F. Wu, G. Chem, J. Phys. Chem. B **108**, 18547 (2004)
8. G.M. Song, W.J. Li, Y. Zhou, Mater. Chem. Phys. **87**, 162 (2004)
9. D. Capsoni, M. Bini, G. Chiodelli, V. Massarotti, P. Mustarelli, L. Linati, M.C. Mozzati, C.B. Azzoni, Solid State Commun. **126**, 169 (2003)
10. A. Eft ekhari, A.B. Moghaddam, B. Yazdani, F. Moztarzadeh, Electrochim. Acta **52**, 1491 (2006)
11. H.W. Liu, K.L. Zhang, Mater. Lett. **58**, 3049 (2004)
12. S. Chitra, P. Kalyani, T. Mohan, R. Gangadharan, J. Electroceram. **3**, 433 (1999)
13. Y.S. Lee, Y. Hideshima, Y.K. Sun, M. Yoshio, J. Electroceram. **9**, 209 (2002)
14. D. Singh, W.-S. Kim, V. Craciun, H. Hofmann, R.K. Singh, Electrochem. Solid-State Lett. **5**(9), A198 (2002)
15. S.B. Tang, M.O. Lai, L. Lu, S. Tripathy, J. Solid State Chem. **179**, 3831 (2006)
16. M.A. Camacho-Lopez, L. Escobar-Alarcon, E. Haro-Poniatowski, C. Julien, Mat. Res. Soc. Symp. **617**, J3.17.1 (2000)
17. Y. Xia, T. Sakai, T. Fujieda, X.Q. Yang, X. Sun, Z.F. Ma, J. McBreen, M. Yoshio, J. Electrochem. Soc. **148**(7), A723 (2001)
18. Y.P. Wu, E. Rahm, R. Holze, Electrochim. Acta **47**, 3491 (2002)
19. C.M. Julien, M. Massot, C. Poinsignon, Spectrochim. Acta Part A **60**, 689 (2004)
20. C.M. Julien, M. Massot, Mater. Sci. Eng. **B97**, 217 (2003)